Optics and Lasers in Engineering 134 (2020) 106309

Contents lists available at ScienceDirect

Optics and Lasers in Engineering

journal homepage: www.elsevier.com/locate/optlaseng

An eave-like model for the welding of 304 stainless-steel tailor-welded blanks with different thicknesses

Hongbo Zhu[a,d,1], Bo Cheng[b,1], Guangyi Ma[b], Xingchen Lin[a,c,*], Yawei Zhang[a], Dongjiang Wu[b], Yongqiang Ning[a,d], Lijun Wang[a,d]

[a] State Key Laboratory of Luminescence and Applications, Changchun Institute of Optics, Fine Mechanics and Physics, Chinese Academy of Sciences, Changchun 130033, China
[b] Key Laboratory for Precision and Non-traditional Machining Technology of Ministry of Education, Dalian University of Technology, Dalian, 116024, China
[c] Science College, Harbin Engineering University, No.145, Nantong Road, Harbin 150001, China
[d] Center of Material Science and Optoelectronics Engineering, University of Chinese Academy of Sciences, Beijing 100049, China

ARTICLE INFO

Keyword:
Laser welding
Diode laser processing
Stainless steel
Tailor-welded blanks
High-temperature ferrite

ABSTRACT

Due to its excellent corrosion resistance and machinability, stainless-steel material has been widely used in many different areas, such as nuclear power and the aircraft industry. In these applications, the stainless-steel parts often consist of tailor-welded blanks with different thicknesses. It is crucial to keep the tailor-welded blanks of high quality in order to satisfy the demanding requirements. To make the welding process of tailor-welded blanks simple and efficient, a novel welding model for the eave-like structure is proposed in this paper. Based on this model, the butt welding of tailor-welded blanks with a plate thickness combination of 2.0 mm and 1.0 mm are successfully completed by high power diode laser sources. For further inspecting the performance of the welded bead, we analyze the microstructure and evaluate the mechanical strength. The results prove that our tailor-welded blanks can satisfy the industrial requirements. This work gives an experimental guide on the welding of tailor-welded blanks with different thicknesses.

1. Introduction

Tailor-welded blanks (TWBs) are the collective of semi-finished metal sheet products which are made from two thin metal plates with different thicknesses or materials [1,2]. TWBs with different thicknesses are cost-effective and environment-friendly solutions, which can also benefit weight reduction in industrial applications. In so many joining technologies for TWBs, laser welding has been proved to be a promising method because of its high energy density, lower heat input, and precise control of the processing region [3–5]. Over the past years, several research communities have investigated the fabrication method for TWBs. Chan et al. studied the effects of different thickness ratio on forming limit diagrams. In their research, SPCC steel sheets with thickness ratios of 2, 1.67, and 1.25 are welded by a 1450 W Nd:YAG laser [6]. Hideki et al. reported that the butt joint welding of TWBs with a plate thickness combination of 2.0 mm and 0.8 mm is realized using a 5 kW CO_2 laser system with an applied electrical potential [7]. In previous works, TWBs with different thicknesses are all formed by the laser butt welding, in which two metal plates of the vertical edge and of different thicknesses are precisely set for welding. This method requires high edge quality and butt-joint accuracy, otherwise, the rosin joint and defects will occur in the weld bead. Therefore, it must increase the complexity of the processing and decrease the production yield. However, scientists have mainly focused on the demonstration of the welding of TWBs composed by dissimilar materials in the last decade [8,9], and the concerned new theory and welding model for solving the above issues have rarely been investigated. In this paper, a novel welding model of the eave-like structure for the welding of TWBs with different thicknesses is proposed to tackle these issues. We also perform the corresponding experimental investigations. Based on this new welding model, the butt welding of 304 stainless steel (304SS) TWBs with a plate thickness combination of 2.0 mm and 1.0 mm is successfully demonstrated using diode laser sources. It is well-known that 304SS has the advantage of corrosion resistance and machinability. Due to its excellent properties, 304SS is widely used in many different areas, such as aerospace, nuclear energy, and heat exchanger [10,11]. However, it tends to induce carbide precipitation, thermal cracks, and other problems in the welding process of the 304SS material [12]. Therefore, novel methods to better the fabrication process of TWBs with different thicknesses are highly desired. This new model and the experimental investigations shed new light on high-quality welding of 304SS TWBs.

* Corresponding author.
E-mail address: lxcciomp@163.com (X. Lin).
[1] These authors contributed equally to this work

https://doi.org/10.1016/j.optlaseng.2020.106309
Received 21 April 2020; Received in revised form 10 July 2020; Accepted 16 July 2020
Available online 21 July 2020

Table 1
The chemical composition of 304SS.

Material	Ni	Fe	Cr	Mo	W	Co	Mn	C	Si	P	S
304SS		Bal					≤	≤	≤	≤	≤0.03

2. Experimental principle and procedures

2.1. Experimental principle

Fig. 1 diagrammatically explains the processing principle of this new welding model. First of all, a laser beam with an incident angle of 10° relative to the vertical direction is utilized to obliquely cut the thin and thick metal plates. This operation is mainly for making an inclined edge on the metal plates. Then, precut metal plates with different thicknesses are butt jointed, which can form an eave-like structure. Lastly, when a laser beam is focused on the marginal area of the thick plate, the molten metal flows into the gap and welds two plates together. The molten metal can produce similar effects as the welding wire so that we call this method "similar filler wire welding". Theoretically, the marginal area of the thick plate could absorb all the laser energy. Therefore, the beam loss and the rosin joint in the traditional welding procedure are avoided in our method.

2.2. Experimental procedures

In the experiment, 304SS metal plates with thicknesses of 1 mm and 2 mm are prepared as the base metal for fabricating TWBs. The chemical composition of 304SS is listed in Table 1. Before the welding, metal plates are machined to rectangles with a size of 200 mm × 100 mm and then milled to remove the oxidized film. The milled plates are ultrasonically cleaned with acetone and then dried for processing.

The diode laser source (DLS) is applied in the welding process due to its shorter wavelength compared to other laser sources, which could relieve problems associated with welding highly reflective materials, such as stainless steel and aluminum [13]. According to the processing requirement described above, two DLSs developed in our lab with the output power of 1 kW and 2 kW are employed for precutting and welding, respectively. These two DLSs, developed by the technology of dense spectral multiplexing, can yield 91x nm, 94x nm and 97x nm. Details with regard to the design and the characteristics of this diode laser source are presented in [14]. Meanwhile, optical fibers are connected to the cutting head and the welding head, respectively [14,15]. These two DLSs are integrated into a cutting machine. Both the cutting head and the welding head are mounted on a 3D motion system which can motion toward X, Y and Z direction. Optical parameters of both DLSs and laser processing heads as well as experimental parameters of the laser processing are presented in Table 2. To achieve high-quality TWBs welding, the precut edge should be well-processed without any burrs. Thus, a set of standard parameters for laser cutting with 1 μm fiber lasers are used in the precutting [16]. The nozzle diameter is 2 mm, and the assistant cutting gas is N_2, and the flow rate is 20 L/min. To obtain the optimal achievable cutting results, the focal point position is adjusted to the middle of 304SS metal plates during the cutting process. Using this set of parameters, 304SS metal plates are successfully cut. The roughness of the cut surface is approximately Rz = 20 μm. From my point of view, although the roughness is higher than that of our case, it will not affect the welding. This point is greatly advantageous over the traditional welding of TWBs with the vertical edge.

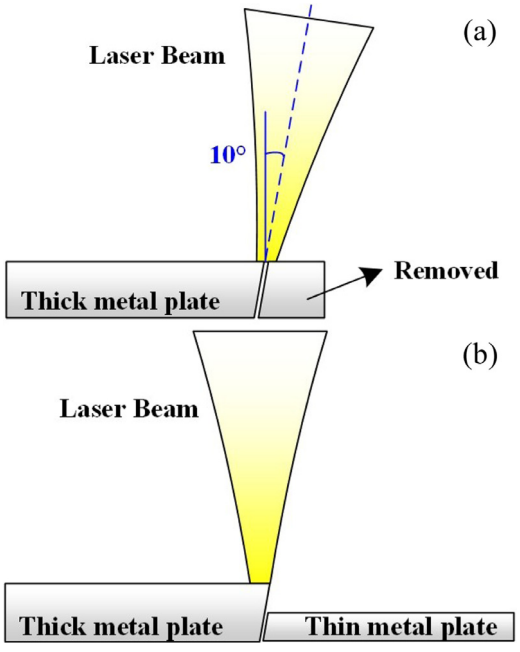

Fig. 1. Schematic of an eave-like model for the welding of TWBs. (a) Precutting. (b) Welding.

Table 2
Optical parameters of both DLSs and laser processing heads as well as the experimental parameters of the laser processing.

Parameters	1 kW DLS for cutting	2 kW DLS for welding
Power	1000 W	2000 W
Wavelength	9xx nm	9xx nm
Fiber core diameter	100 μm	200 μm
Processing head	Cutting head	Welding head
Collimating Lens*	100 mm	100 mm
Focusing Lens*	125 mm	200 mm
Focus spot	125 μm	400 μm
Nozzle diameter	2 mm	–
Nozzle distance	0.5mm	–
Processing speed	5 m/min	3 m/min
Assistant gas	N_2	N_2
	20 L/min	20 L/min

* Optical lenses in the processing heads are coated by antireflective films with a residual reflectance of 0.3%.

Many welding experiments of TWBs are performed according to the above processing procedure. We visually inspect welded TWBs and select eligible ones for microstructure analysis. To conveniently investigate the microstructure, welded TWBs are firstly machined into small samples using a wire-electrode cutting machine. Then, the weld bead of these TWBs are milled by 240#, 360#, 600#, 800#, 1000#, 1200#, 1500#, 2000# sandpapers, and polished by SiC grinding paste. Finally, the dilute aqua regia is applied for metallographic corrosion.

3. Results and discussion

3.1. The cross-section profile and element analysis

The cross-section profile of the weld bead is inspected by an optical microscope (OM). The OM image of the cross-section is shown in Fig. 2. We can see that the weld bead is free from cracks and pores. In addition, the transition zone is very smooth.

Fig. 3 shows element distributions in the weld bead, which is detected by an energy dispersion spectrometer (EDS) and an electron probe micro-analyzer (EPMA). Because the laser welding features rapid melt-

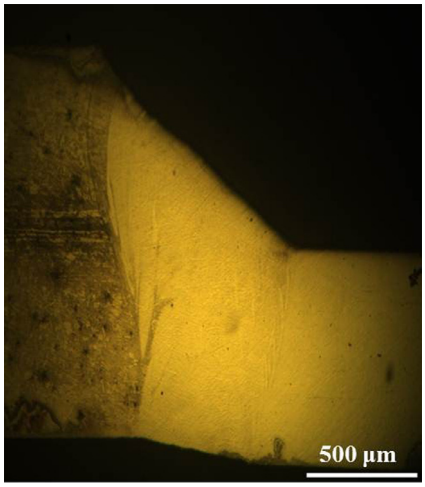

Fig. 2. The cross-section profile of the weld bead.

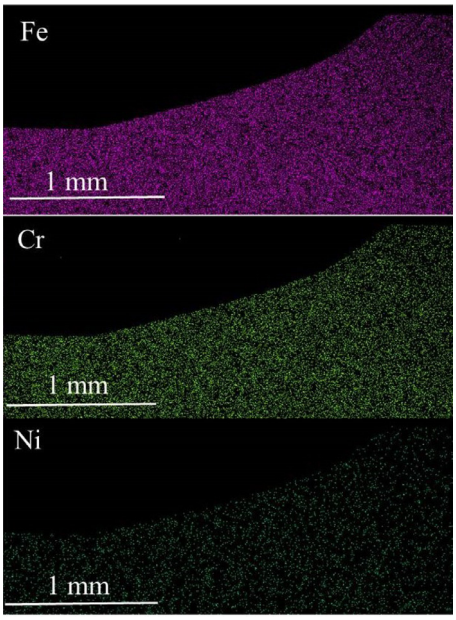

Fig. 3. Distribution of main elements in the weld bead.

ing and solidification, main elements throughout the weld bead display a uniform distribution. The element content is almost unchanged compared with that in the base material. Besides, the fusion line of the weld is not obvious, which indicates no element burning occurs in the weld bead. The EPMA line scanning results of the welded sample are plotted in Fig. 4. As shown in Fig. 4, the element distributions in the weld bead are similar to that in the base material, which further confirms no element burning occurs in this process, especially for Cr element. Furthermore, horizontal fluctuations of both Cr and Fe element distributions are also consistent with that in the base metal. Nevertheless, it is worth noting that the index of Ni element distribution is significantly higher than that in the base material, which can be attributed to the different solubility of Ni element in the austenite and ferrite.

3.2. Microstructure characteristics

The microstructure of the weld bead is analyzed by scanning electron microscope (SEM) equipped with EDS. The microstructure at different parts of the weld bead is illustrated in Fig. 5. As shown in Fig. 5, the fusion transition zone and the fusion zone constitute the macrostructure of

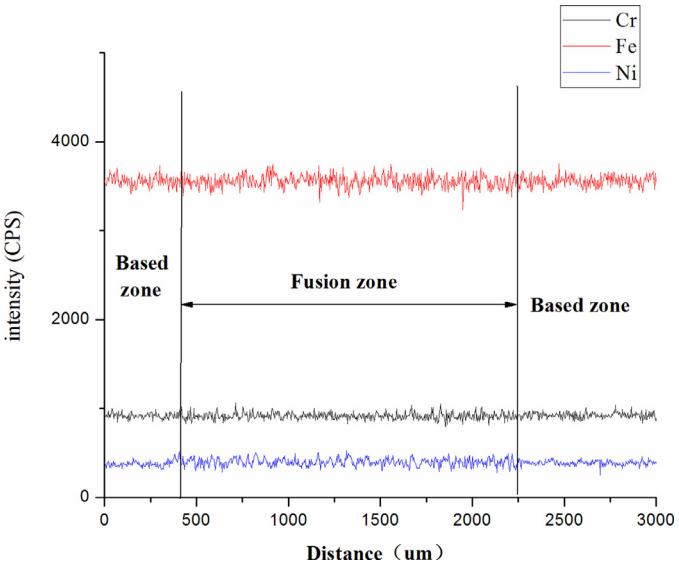

Fig. 4. EPMA line scanning of the welded sample.

the weld bead. From the microscopic viewpoint, the microstructure of the weld bead mainly consists of the austenite and the ferrite, wherein the ferrite falls into two categories: the skeleton ferrite and the strip ferrite. The closer to the center of the weld bead, the less content of strip ferrite and the more content of skeleton ferrite. Moreover, the fusion transition zone of base metal is composed of skeleton ferrite and equiaxed austenite. Comparing Fig. 5b with Fig. 5d, it can be found that the fusion transition zone close to the thin plate is broader than that close to the thick plate, which is due to the poor thermal dissipation of the thin plate. Fig. 6 shows the detection of the grain orientation in the weld bead and base material by electron back scattered diffraction (EBSD). As shown in Fig. 6, the grain in the weld bead presents the feature of epitaxial growth. There is no noticeable grain enlargement at the interface of the weld bead and the base material, indicating no obvious heat affected zone. Besides, grains in the thin plate have a larger size, which is mainly due to the poor thermal dissipation and the slow cooling rate of the thin plate.

The phase composition in the weld bead is investigated by X-ray diffraction (XRD), which is plotted in Fig. 7. Obviously, the result further demonstrates that the microstructure of the weld bead indeed consists of the austenite and the ferrite. The volume fraction of the ferrite in the weld bead is largercompared with that in the base metal.

Generally speaking, the microstructure and the solidification path of stainless-steel material are evaluated by the Creq/Nieq ratio [17,18]. The Creq/Nieq ratio of 304 austenitic stainless steel is 1.82. Hence, the corresponding solidification mode of the weld bead is FA mode [18]. In this mode, the ferrite is formed during the initial period of the weld bead solidification. Then, the ferrite phase has a peritectic-eutectic reaction at the end of the solidification process, which leads to the generation of the austenite phase. The rapid cooling rate of the laser welding restrains the transformation of the ferrite phase to the austenite phase. Hence, the high-temperature ferrite (δ - ferrite) is retained. That is why the volume fraction of the ferrite in the weld bead is larger compared with that in the base metal. As we know, the high-temperature ferrite usually has higher solid solubility, whereby it gains higher strength. Based on the above EDS and EPMA detection, the main elements uniformly distribute in the weld bead, which shows that the Creq/Nieq ratio is unchanged with the position of the weld bead. Thus, the variation of the microstructure in different locations is a consequence of the different local cooling rate. Detailed illustrations are as follows.

- The cooling rate of the fusion transition zone is faster, and correspondingly, the constitutional supercooling is higher. which results

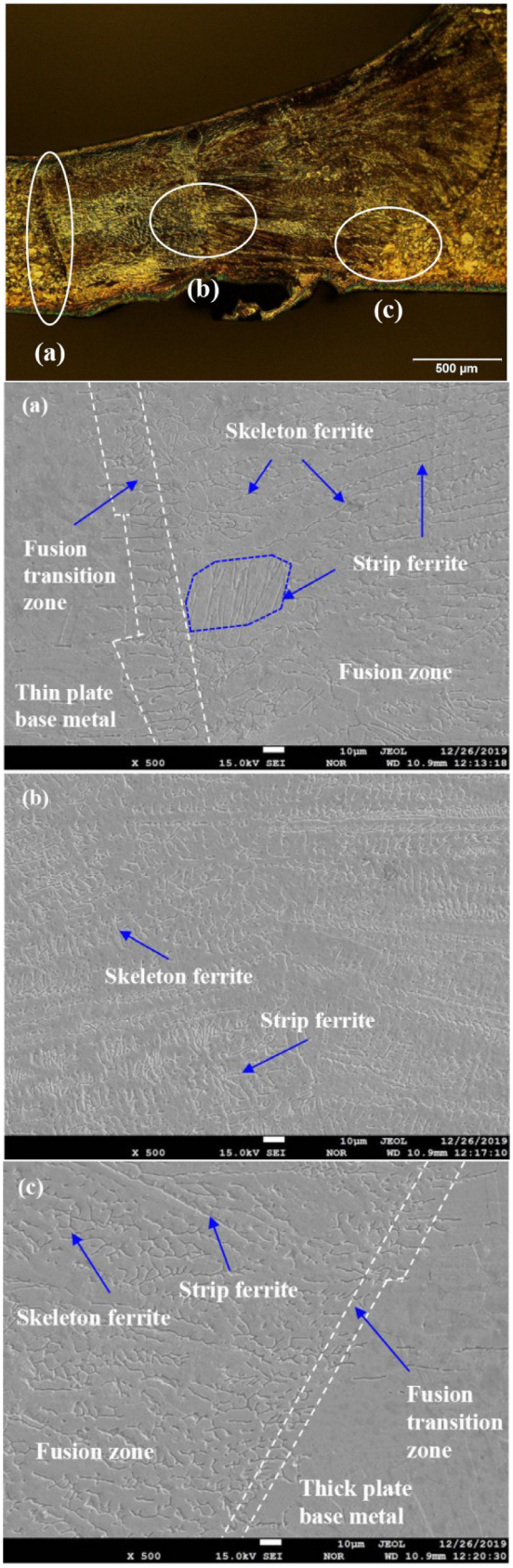

Fig. 5. Microstructure at different parts of the weld bead.

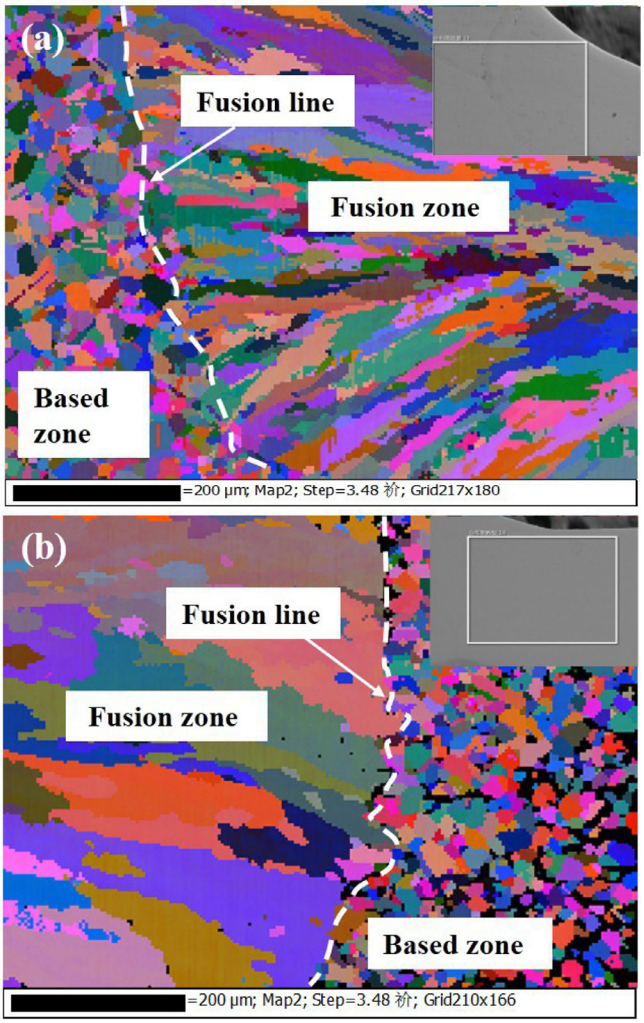

Fig. 6. Grain orientation diagram, a) the interface between thick plate and fusion zone, b) the interface between thin plate and fusion zone.

in the microstructure of the weld bead to be composed of the fine equiaxed austenite and the skeleton ferrite.

- The temperature gradient at the junction of the base metal and the weld bead is large, which tends to generate the ferrite at the initial period of the weld bead solidification. On the other hand, since the rapid cooling rate of this region can restrain the transformation of δ to γ, the coarse ferrite frame is retained to form the strip ferrite. Therefore, the volume fraction of the ferrite in this region is high.

Comparing with the fusion transition zone, the cooling rate of the weld bead center is slower, so the transformation of δ to γ is sufficient. Meanwhile, the temperature gradient in this region is small, so the volume fraction of the ferrite is reduced, wherein the residual ferrite is mainly skeleton ferrite. Furthermore, the primary microstructure here is the equiaxed austenite because of the high constitutional supercooling.

3.3. Tensile strength test

The tensile strength test is performed to evaluate the strength of TWBs. TWBs for tensile strength test are cut to specimens with a "dog-bone" shape by a wire-electrode cutting machine. The size of specimens is shown in Fig. 8. At room temperature, three tensile strength tests are carried out by a tensile testing machine with a tensile rate of 5 mm/min. Curves of the strength with the displacement of specimens are plotted

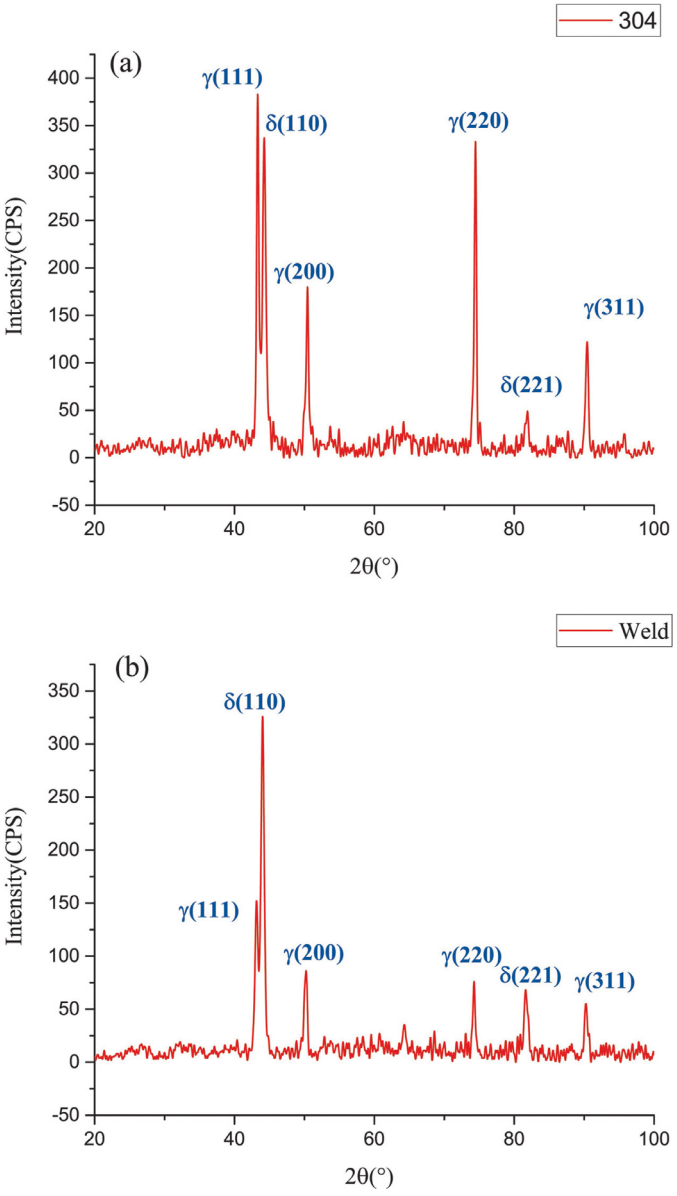

Fig. 7. XRD pattern of the base metal a) and the weld bead b). γ is the austenite, and δ is ferrite.

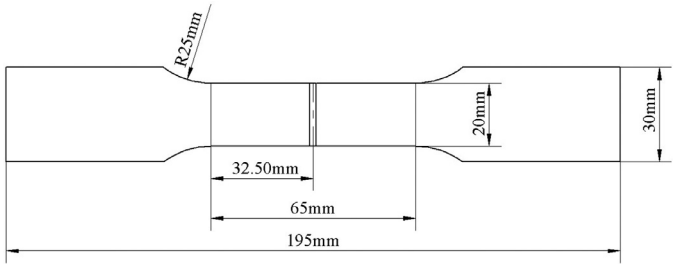

Fig. 8. Dimensional drawing of tensile test specimens.

in Fig. 9. In these tests, all specimens fracture at the thin base metal plate. From the cross-section profile of the weld bead we can find that the depth of fusion in the weld bead is deeper than that in the thin metal plate. Furthermore, the increase of the residual high-temperature ferrite will improve the strength of the weld bead [19]. At the same time, the rapid cooling rate of the laser welding renders the grain fine. Due to

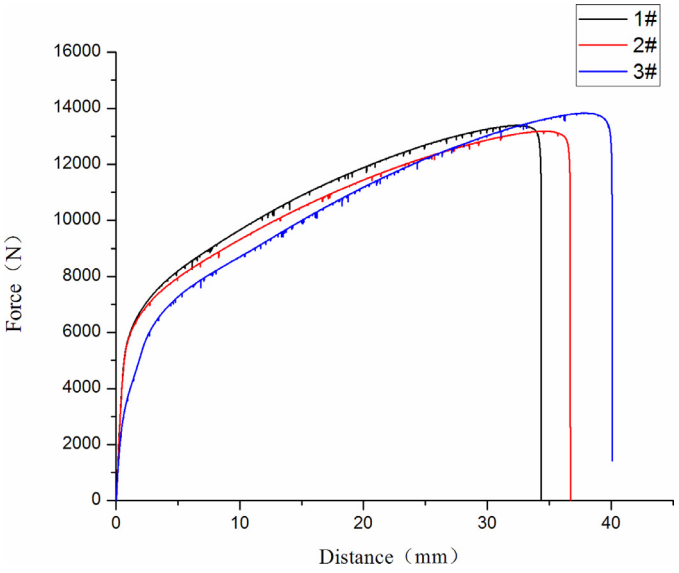

Fig. 9. Curves of the strength with the displacement of specimens.

the above reasons, the strength of TWBs is higher than the base metal, which can explain why specimens fracture at the base metal.

4. Summary and conclusions

In this work, a novel welding model of the eave-like structure for the welding of TWBs with different thicknesses has been introduced and demonstrated. Based on this new welding model, high-quality butt welding of 304SS TWBs with a plate thickness combination of 2.0 and 1.0 mm is achieved. Results of the microstructure analysis and the tensile strength test show that the welded TWBs can satisfy the requirement of industrial applications. This welding method is promising to simplify the processing procedures and improve production efficiency.

Declaration of Competing Interest

The authors declare that they have no known competing financial interests or personal relationships that could have appeared to influence the work reported in this paper.

Acknowledgement

This work was supported by the National Natural Science Foundation of China (NSFC) (61674149) and National Key Research and Development Program of China (2017YFB1104400).

References

[1] Xiaohu H, Honggang D, Yueqing X, et al. Microstructure and mechanical properties of laser welded TC4 titanium alloy/304 stainless steel joint with $(CoCrFeNi)_{100-x}Cu_x$ High-entropy ally interlayer. J Alloys Compd 2019;803:649–57.
[2] Marion M, Maren J, Michael L, et al. A review on tailored blanks-Production, applications and evaluation. J Mater Process Technol 2014;214:151–64.
[3] Jack A, Bernd B. Diode laser welding of stainless steel 304 L.. J. Mater Process Technol 2017;240:138–44.
[4] Xingchen L, Pengfei W, Yawei Z, et al. Theoretical and experimental aspects of laser cutting using direct diode laser source based on multi-wavelength multiplexing. Opt Laser Technol 2019;114:66–71.
[5] Bauke W T, Mario M, Christian AZ. Recent advances in ultrafast semiconductor disk lasers. Light: Sci Appl 2015;4:e310.
[6] Chan S M, Chan L C, Lee T C. Tailor-welded blanks of different thickness ratios effects on forming limit diagrams. J Mater Process Technol 2003;132:95–101.
[7] Hideki H, Yasunobu M, Maschiro O. Effect of applying electrical potential to a CO_2 laser welding of different thickness plates. Sci Technol Adv Mater 2005;6:712–19.
[8] Gang S, Taotao L, Zhaodong Z, et al. Investigation of unequal thickness Mg/steel butt-welded plate by hybrid laser-tungsten inert gas welding with a Ni interlayer. J Manuf Process 2017;30:299–303.

[9] Gang L, Xiaofeng L, Xiaolei Z, et al. Fiber laser butt joining of AZ 31B alloy to 304 stainless steels with copper foil. Opt Laser Technol 2019;117:215–26.
[10] Yunfei M, Xinwei L, Ming G, et al. Microstructures and mechanical properties of laser-arc hybrid welded dissimilar pure copper to stainless steel. Opt Laser Tchnol 2019;111:140–5.
[11] Gang L, Xiaofeng L, Xiaolei Z, et al. Fiber laser butt joining of AZ31B alloy to 304 stainless steels with copper foil. Opt Laser Tchnol 2019;117:215–26.
[12] Balachandar K, Manideep D. Welding parameters-metallurgical propertoes correlation frictionwelding of austenitic stainless steel and ferritic stainless steel. J Appl Sci 2012;12:1013–19.
[13] Yi S, Kun Z, Meixin F, et al. Room-temperature continuous-wave electrically pumped InGaN/GaN quantum well blue laser diode directly grown on Si. Light: Sci Appl 2018;7(13).
[14] Hongbo Z, Xingchen L, Yawei Z, et al. kW-class fiber-coupled diode laser source based on dense spectral multiplexing of an ultra-narrow channel spacing. Opt Express 2018;26:24723–33.
[15] Hongbo Z, Shengli F, Jian Z, et al. Development and thermal management of kW–class high-power diode laser source based on the structure of two-stage combination. IEEE Photonics J 2019;11:1502510.
[16] Witte U, Schneider F, Traub M, et al. kW-class direct diode laser for sheet metal cutting based on DWDM of pump modules by use of ultra-steep dielectric filters. Opt Express 2016;24:22917–29.
[17] Suutala N, Takalo T, Moisio T. The relationship between solidification and microstructure in austenitic and austenitic-ferritic stainless steel welds. Metall Mater Trans A 1979;10:512–14.
[18] Kadoi K, Shinozaki K. Effect of chemical composition on susceptibility to weld solidification cracking in Austenitic weld metal. Metall Mater Trans A 2017;48A:5860–9.
[19] Kulkami A, Dwivedi D, Vasudevan M. Dissimilar metal welding of P91 steel-AISI 316 L SS with Incoloy 800 and Inconel 600 interlayers by using activated TIG welding process and its effect on the microstructure and mechanical properties. J. Mater. Process. Technol 2019;274:116280.